Photoexcited carrier relaxation dynamics and terahertz response of photoconductive antennas made on proton bombarded GaAs materials

Cite as: J. Appl. Phys. **108**, 124507 (2010); https://doi.org/10.1063/1.3524539
Submitted: 10 August 2010 . Accepted: 02 November 2010 . Published Online: 28 December 2010

S. Savard, J.-F. Allard, M. Bernier, J. C. Petersen, J. S. Dodge, P. Fournier, and D. Morris

Photoexcited carrier relaxation dynamics and terahertz response of photoconductive antennas made on proton bombarded GaAs materials

S. Savard,[1,2] J.-F. Allard,[1] M. Bernier,[1] J. C. Petersen,[2] J. S. Dodge,[2,3] P. Fournier,[1,3] and D. Morris[1,a)]

[1]*Département de physique, Regroupement Québécois sur les Matériaux de Pointe, Université de Sherbrooke, Québec J1K 2R1, Canada*
[2]*Department of Physics, Simon Fraser University, Burnaby, British Columbia V5A 1S6, Canada*
[3]*Canadian Institute for Advanced Research, Toronto, Ontario M5G 1Z8, Canada*

(Received 10 August 2010; accepted 2 November 2010; published online 28 December 2010)

We present a model reproducing the instrumental response of a time-domain spectrometer that integrates photoconductive transmitter and receiver antennas made on identical proton-bombarded GaAs substrates. This model is used to determine the ultrafast capture time of the photoexcited carriers by the ion-bombardment-induced traps. A 0.5 ps capture time can be extracted for a low laser pump fluence of 0.66 $\mu J/cm^2$ per pulse. This carrier trapping time gets longer as the pump fluence increases. This behavior is explained by a gradual filling of the traps that are distributed over a 1 μm depth from the GaAs surface. This interpretation is supported by time-resolved measurements obtained on the same photoconductive material using both an 820 nm pump/terahertz-probe transmission experiment and a degenerate 760 nm pump/probe reflectivity experiment. The differential transmission and reflectivity dynamics are reproduced using a biexponential function which correctly describes the photoexcited carrier relaxation and transport dynamics in this material. The strong agreement observed between these different measurements reinforces the validity of the theoretical model used to reproduce the instrumental response of the terahertz setup. © *2010 American Institute of Physics*. [doi:10.1063/1.3524539]

I. INTRODUCTION

Photoconductive materials triggered by ultrafast laser pulses are often used to generate and detect ultrashort electrical transients.[1] Photoconductive (PC) low-aperture antennas combined with a silicon lens are now commonly used in freely propagating wave terahertz spectroscopy systems since they produce well-collimated beams and offer a good signal to noise ratio over a range of frequencies from 0.1 to 5 THz. The emergence of several spectroscopic and imaging applications in the terahertz (THz) frequency regime[2] demands the continued development of high-performance and low-cost emitters and detectors. Ion-implanted silicon-on-sapphire (SOS) (Ref. 3) has long been a material of choice for making THz antennas since the fabrication process is simple, reproducible and inexpensive. Low-temperature (LT) grown GaAs film is particularly attractive since it presents good electrical properties such as high dark resistivity, high carrier mobility and short carrier lifetime.[4–6] The optical and electrical breakdown thresholds are also much higher in LT-GaAs than in standard semi-insulating GaAs or silicon. The widespread use of this material is, however, limited by the cost of the epilayer. More recently ion-implantation into III-V semiconductors followed by thermal annealing has become an alternative fabrication process, producing PC THz antennas with high figures of merit.[7–10] Their optical and electrical breakdown thresholds approach those of LT-GaAs.[11] Among the different ion species that could be used, protons (H^+) are very attractive since it is relatively easy to control the depth of the induced defects using a low-energy ion-implanter. PC antennas made this way have reproducible characteristics and the overall process is relatively inexpensive. This method also offers spatial selectivity that could be used to fabricate more complex photonic devices like those integrating a THz emitter, waveguide, and detector on the same chip.

Further optimization of the ion-implantation and thermal annealing process relies on our capability to understand how the structural changes are affecting the PC antenna characteristics, especially the THz response. The basic physics of ultrafast semiconductor switches is relatively well understood.[1] The time-dependent response functions of PC THz emitters and detectors are related to the temporal behavior of the photocurrent which itself is mainly governed by the carrier scattering time (τ_s) and trapping time (τ_c).[12–14] The overall response function of a time-domain THz spectroscopy system is often complicated by the influence of experimental conditions such as the laser excitation density, dimension of the detecting area and imaging characteristics of the optical system used to relay the pulses from the source through the sample to the detector. In modeling the spectrum of the instrumental THz pulses (designated as reference pulses) researchers often rely on independent determination of the characteristic relaxation times using time-resolved optical measurements. Several recent studies[15–19] have investigated the physics underlying the PC antenna characteristics but there is still a need to establish a strong link between the THz instrumental response function (spectrum of the reference THz pulses) and the relaxation times extracted from time-resolved pump-probe measurements. Such a compari-

a)Electronic mail: denis.morris@usherbrooke.ca.

son will fix the limits of validity of the models used for data analysis and more broadly it will be useful to better understand the influence of ion-bombardment conditions on the resulting changes of the PC antenna characteristics without resorting to complementary characterization measurements.

In this article, we describe our investigation of ultrafast photoexcited carrier relaxation dynamics in proton-bombarded GaAs using three experimental techniques. We used the material as the antenna substrate in a time-domain terahertz spectrometer, and from the spectrum of the measured THz pulses, estimated carrier scattering and trapping times according to a model that will be described in detail. We also determined the trap-induced capture time for photoexcited carriers using an 820 nm pump/terahertz-probe differential transmission experiment and a degenerate 760 nm pump/probe differential reflectivity experiment. A strong correlation was found between the recombination times extracted by the different techniques although the ones extracted from 820 nm pump/terahertz-probe measurements are systematically higher. We also investigated the effect of the laser pump fluence, both on instrumental response function of our time-domain THz spectrometer and on pump-probe measurements, and observed behavior which is well explained by a gradual filling of the traps that are distributed over a 1 μm depth from the GaAs surface.

II. EXPERIMENTS

Commercial high-resistivity ($>10^7$ Ω cm) (100)-oriented semi-insulating SI-GaAs substrates were used as starting materials. These substrates were first bombarded with protons of 50 keV, 100 keV, and 150 keV at doses of 0.5 ions/cm^2, 1 ions/cm^2, and 3.5×10^{15} ions/cm^2, respectively. This process generated a distribution of nonradiative decay centers corresponding to 5×10^{20} traps/cm^3 in a region extending 1 μm from the surface. The ion-implantation process was followed by thermal annealing at 500 °C for 20 min under N_2 gas using a GaAs cap to prevent As desorption. These proton-damaged GaAs substrates were used to fabricate ultrafast photoconductive antennas, also known as Auston switches.[20] The emitter and detector were made from the same implanted substrate. Ohmic contacts were created using a standard mixture of Ni/Au–Ge/Au for the metallization followed by rapid annealing at around 410 °C for 30 s. The coplanar electrodes of the emitter and detector are separated by gaps of 120 μm and 30 μm, respectively. Each electrode is 10 μm wide, 12 mm long for the emitter, and 6 mm long for the detector. A 50 V bias voltage is applied to the PC antenna emitter.

A mode-locked Ti:sapphire laser at a repetition rate of 82 MHz was used as the excitation source for the generation of broadband pulsed THz radiation in the time-domain terahertz spectrometer (THz-TDS). The laser wavelength was centered at 760 nm and the duration of the optical pulses was about 120 fs. At 760 nm, we estimate the optical penetration depth of optical pulses in GaAs to be about 500 nm. The excitation beam was focused near the anode of the antenna, into a spot of about 70 μm; a $1/e$ intensity fall criteria is used to define the spot diameter. The laser power was varied in order to vary the fluence, with the maximum fluence being about 16 μJ/cm^2; this would give an average photocarrier density of about $6\times10^{+17}$ electron-hole pairs/cm^3 over the first 500 nm from the surface. The intensity of this pump beam was modulated at a frequency of 3 kHz using a mechanical chopper. A 4 mm diameter hemispherical silicon lens was fixed with silicone grease on the backside of the emitter and detector substrates. The terahertz radiation was collected over a large solid angle and refocused on our detector using these Si lenses combined with a pair of off-axis parabolic mirrors. The electric field of the THz pulses was probed using the detector antenna, gated by pulses from the same laser, subject to a variable delay in order to obtain the time profile of the THz field. The laser power of the probing beam was about 15 mW focused on a 40 μm spot size, covering the entire region between the detector electrodes. A low-noise current preamplifier and a lock-in amplifier were used to retrieve the THz signal. The spectra of the THz traces were then obtained using numerical Fourier transforms.

An 820 nm pump/terahertz-probe system was also used to investigate the carrier relaxation dynamics of the same GaAs substrate. A Ti:sapphire regenerative amplifier (Spitfire model from Spectra-Physics) was used as the laser excitation source. It operates at a repetition rate of 1 kHz generating 60 fs pulses at a center wavelength of 820 nm. The maximum power used for the pumping beam was 8 mW. This beam was weakly focused on the sample surface into a spot diameter of about 7.5 mm which gives a maximum laser fluence of 18 μJ/cm^2 per pulse. The terahertz probe beam was generated by optical rectification in a 2 mm ZnTe crystal and focused onto the sample surface with a spot size of about 3 mm. The transmitted THz pulses were detected using electro-optic sampling in a second crystal of ZnTe, 0.5 mm thick.

Complementary time-resolved optical measurements were also obtained using a degenerate 760 nm pump/probe differential reflectivity experiment. This pump-probe setup uses the same 82 MHz Ti:sapphire oscillator as the one used for the antenna-based spectrometer. The pump and probe beams are focused on the sample surface to a spot size of about 100 μm and 50 μm, respectively. The pump and probe beams are noncollinear and orthogonally polarized. The pump beam is modulated at 1 kHz and this induces a modulation of the reflected probe beam that is detected using a fast Si photodiode and a lock-in amplifier. The laser fluence of the probe beam is at least 100 times smaller than that of the pump beam and we have verified that the dynamics of the temporal reflectivity signals are unaffected by the probe fluence.

III. MODEL

A. Instrumental response of GaAs PC antenna-based THz spectrometer

The far-field amplitude of the electric field $E_g(t)$ generated by the PC antenna emitter is proportional to the first time-derivative of the photocurrent $J(t)$,[1] which is itself given by the convolution of the laser pulse $L(t)$ with the

response function of the emitter $R_e(t)$. In frequency space, this can be simply written as a product of frequency-dependent functions, as follows:[21]

$$E_g(\omega) \propto \omega \times L(\omega) \times R_e(\omega). \tag{1}$$

On the other hand, the measured current signal delivered by our PC antenna detector is proportional to the convolution of the free-space propagating electric field that reaches the detector $E_d(t)$ with both the laser pulse $L(t)$ and the response function of the detector $R_d(t)$. In frequency space, this can be written as follows:

$$S(\omega) \propto E_d(\omega) \times L(\omega) \times R_d(\omega). \tag{2}$$

The THz electric field measured by the PC antenna detector depends on the field generated at the source, but also on the overall wave-propagating transfer function between the emitter and the detector, as well as the geometry of the detector itself. The apparent spectral content of the THz pulse is modified by the limited aperture of THz optics and the limited area of our detector, which both tend to filter out the low-frequency part of the THz wave-packet.[12,22] We account for this effect by modeling the wave-propagating transfer function as a high-pass filter in the form of a complementary error function (Erfc). The spectrum of pulses detected using the time-domain THz spectrometer can then be written, in frequency space, as follows:

$$S(\omega) \propto \omega \times L^2(\omega) \times R_e(\omega) \times R_d(\omega) \times \mathrm{Erfc}\left[\frac{-(\omega-\omega_{lf})}{\Delta\omega_{lf}}\right], \tag{3}$$

where ω_{lf} is the cut-off angular frequency and $\Delta\omega_{1f}$ the angular frequency spread of the cut-off function. This $S(\omega)$ expression can be designated as the overall instrumental response of the THz spectrometer. We assume that the laser pulse $L(t)$ has a Gaussian envelope with full width at half maximum Δt_l, and is Fourier-transform-limited. The corresponding function in frequency space is written as follows:

$$L(\omega) \propto \exp\left[-\frac{(\omega \times \Delta t_l)^2}{16 \times \ln(2)}\right]. \tag{4}$$

In deriving the form of the response function $R(t)$, we neglect the effect of time-dependent screening, an approximation which should be valid for low fluence. Piao *et al.*[13] have showed that this effect has a negligible impact on the THz waveform generated for a carrier excitation density smaller than 1×10^{18} cm^{-3} although other authors have found that the onset of saturation of the emitted THz radiation, due to radiation field screening,[23] occurs at around 1×10^{17} electron-hole pairs per cubic centimeter. Considering a Drude-type expression for the carrier mobility that enters into the photocurrent expression, the causal response function $R(t)$ can be written as follows:[24]

$$R_e(t), R_d(t) \propto \theta(t) \times \left(\frac{\tau_c}{\tau_c - \tau_s}\right) \times (e^{-t/\tau_c} - e^{-t/\tau_s}), \tag{5}$$

where $\theta(t)$ is a step function, τ_s is the carrier scattering time, and τ_c is the carrier capture time by the ion-implanted induced traps. We assume in this model an average lifetime for all carriers contained in the photoexcited region, and no diffusion toward the undamaged bulk region of the substrate. This approximation is valid at low laser fluence where each electron/hole in the spatial distribution of excited carriers is surrounded by an equivalent density of active traps. At high laser fluence on the emitter, one must consider the effect of trap filling, which will cause the carrier diffusion and recombination rates to vary with depth in the substrate. We have used a single carrier recombination time in our model but we will show that these effects tend to increase the averaged carrier capture time and reduce slightly the high-frequency cut-off value of the THz instrumental response function. Considering the limitations of this model, the corresponding response function can be written, in frequency space, as follows:

$$R(\omega) \propto \frac{\tau_c}{(1-i\omega\tau_c) \times (1-i\omega\tau_s)}. \tag{6}$$

In most THz-TDS systems, the THz pulses have to pass through the absorbing and dispersive substrates of both the emitter and detector. For two 0.5 mm thick semi-insulating GaAs substrates, the absorption of THz radiation is significant in the 0.1 to 5 THz frequency range. Grischkowsky *et al.*[25] have observed two weak absorption features at 0.4 and 0.7 THz but the main absorption peak,[26] associated with the infrared-active TO phonon in GaAs, occurs at 8 THz. If we consider the dipole approximation model with a single absorption band centered at $\omega=\omega_0$, we can write the real (ε_1) and imaginary (ε_2) parts of the dielectric function as:

$$\varepsilon_1 = \varepsilon_\infty + (\varepsilon_0 - \varepsilon_\infty) \times \left\{\frac{[1-(\omega/\omega_0)^2]}{[1-(\omega/\omega_0)^2]^2 + (\gamma\omega/\omega_0^2)^2}\right\},$$

$$\varepsilon_2 = (\varepsilon_0 - \varepsilon_\infty) \times \left\{\frac{\gamma\omega/\omega_0^2}{[1-(\omega/\omega_0)^2]^2 + (\gamma\omega/\omega_0^2)^2}\right\}, \tag{7}$$

where ε_0 is the static dielectric constant, ε_∞ is its high-frequency limit, ω_0 is the angular resonance frequency, and γ is the damping rate of the oscillation motion. The real (n) and imaginary parts (κ) of the refractive index can easily be obtained using the relation between the complex dielectric and refractive index functions $(\tilde{n}^2=\tilde{\varepsilon})$. The frequency-dependent absorption function $\alpha(\omega)$ is given by $\alpha=2\kappa\omega/c$, where c is the speed of light. The absorption coefficient and the index of refraction for semi-insulating GaAs are plotted in Fig. 1 as a function of the frequency using the above expressions and empirical values taken from the literature. The refractive index $n(\omega)$ induces a slight modification of the THz waveform while the THz pulse passes through the GaAs antenna substrate but its spectral content is only affected by the frequency-dependent absorption function. Because high-resistivity silicon materials have excellent THz properties in the 0–5 THz frequency range, the absorption and dispersion in the silicon lens of our setup can be ignored. Therefore, the Fourier amplitude of the instrumental (reference) THz pulses can be written as follows:

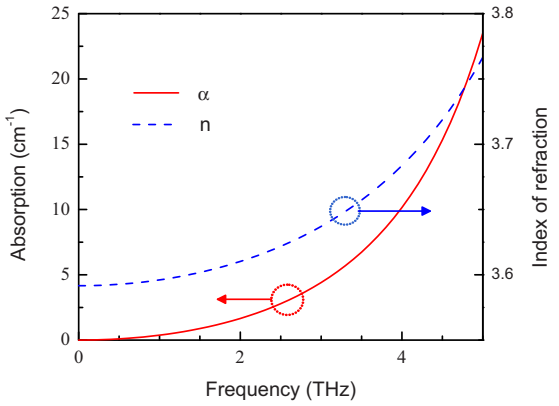

FIG. 1. (Color online) Absorption coefficient (left axis) and index of refraction (right axis) of the semi-insulating GaAs material obtained using the dipole oscillator approximation with a single absorption band. The empirical values used for this plot are $\omega_o = 2\pi \times (8\ \text{THz})$, $\gamma = 2\pi \times (0.2\ \text{THz})$, $\varepsilon_o = 12.9$, and $\varepsilon_\infty = 10.89$.

$$|S(\omega)| \propto \omega \times \text{Erfc}\left(\frac{\omega_{lf} - \omega}{\Delta\omega_{lf}}\right) \times \exp\left[-\frac{(\omega \times \Delta t_l)^2}{8 \times \ln(2)}\right] \times \frac{1}{(1+\omega^2\tau_c^2) \times (1+\omega^2\tau_s^2)} \exp\left(\frac{-\alpha_{\text{GaAs}} \times d}{2}\right), \tag{8}$$

where d is the overall thickness of the SI-GaAs material.

B. Pump-probe experiments

Beard *et al.*[27,28] have developed a comprehensive model for the analysis of transient terahertz photoconductivity measurements in GaAs. A full two-dimensional series of differential transmission THz traces taken at different pump-probe delay times must be acquired in order to extract time-dependent conductivity data, particularly at short pump-probe delay times. Carrier recombination time can be obtained through a simple differential transmission kinetic measured as a function of the pump-probe delay time (called one-dimensional scan) in the limit where the laser pump does not affect the dispersion properties of the substrate. Moreover, for a thin active absorbing film and for a small pump perturbation $[\Delta T(t)/T_0 < 0.1]$, the differential transmission signal $\Delta T(t)$ is simply proportional to the time-dependent conductivity value $\sigma(t)$.[29] When pumping at 820 nm, the mobility is nearly time-independent[28] so the differential transmission signal should follow the temporal behavior of the carrier density $N(t)$. Since the electron mobility is much higher than the hole mobility in GaAs, we can consider that $\Delta T(t)$ is essentially governed by the temporal evolution of the electron density. Beard *et al.*[28] have showed that a non-negligible fraction of photoexcited carriers diffuse and recombine in the bulk of the GaAs substrate ($>1\ \mu$m from the surface) for an excitation pump at 800 nm. Carrier recombination time will be much longer for carriers that recombine in the deep defect-free region of the substrate (at depths greater than 1 μm). Therefore, we have modeled the differential terahertz transmission signal $\Delta T(t)$ using a biexponential function of the following form:

$$\Delta T(t) = \text{Erfc}\left(\frac{-t}{\tau_s'}\right) \times (A_1 \times e^{-t/\tau_{d_1}} + A_2 \times e^{-t/\tau_{d_2}}), \tag{9}$$

where A_1 and A_2 are the amplitudes of the two exponential functions, τ_{d1} is the averaged trapping time of the carriers generated in the ion-bombarded region, and τ_{d2} is the averaged recombination time of those carriers that are generated directly in the undamaged region of the GaAs substrate added to those that can reach this region by diffusion. A complementary error function (Erfc) has been used to reproduce the rising part of the $\Delta T(t)$ signal. The rise time τ_s' is slightly longer than the carrier momentum relaxation time (τ_s) since it depends also on the temporal response of the ZnTe detector. At high pump fluences, the carrier relaxation dynamics is complicated by variation with depth of the filling occupancy of the carrier traps.

For the degenerate 760 nm—pump/probe differential reflectivity experiment, the amplitude of the $\Delta R(t)$ signal mainly comes from the change in the index of refraction induced by the pump beam which depends on band-filling and bandgap renormalization effects as well as free carrier absorption mechanisms. These time-resolved reflectivity measurements are often difficult to interpret since the sign and the shape of the temporal $\Delta R(t)$ signal depend on the excitation and probing wavelength, the excitation density, and the density of active traps.[30–33] By exciting and probing well above the GaAs bandgap energy, the $\Delta R(t)$ signal is less sensitive to carrier cooling processes and we expect to better see the influence of the fast carrier trapping mechanisms. Under conditions where the time-resolved index change is proportional to the density of free carriers, the $\Delta R(t)$ signal can be reproduced using Eq. (9). In comparison with the $\Delta T(t)$ measurements, the $\Delta R(t)$ signal is much more dependent on the density of photocarriers present within the first few tens of nm from the top GaAs surface.

IV. RESULTS AND DISCUSSION

Figure 2(a) shows the THz traces detected by our time-domain THz spectrometer for different laser pump powers incident on the emitter antenna. The traces have been normalized and displaced vertically for clarity. The electric field transients are characterized by a main positive peak and two negative lobes. The narrow envelope of these THz pulses results from the convolution of the ultrafast responses of the source and detector antennas. The specific waveform of the pulses depends on the aberrations of our instrumental setup and is particularly sensitive to ray-tracing through the Si lenses as well as the dispersion of the generated pulses while they travel through two 0.5 mm thick GaAs substrates. The small oscillations following the main THz pulses are mainly due to water vapor absorption lines.

The Fourier amplitudes of the THz traces are plotted in Fig. 2(b). Significant intensity is detected from 100 GHz to 5 THz. The laser power incident on the source antenna has only a small influence on the spectral content of the THz pulses, with the spectrum decreasing more abruptly at high frequencies for the highest laser fluence; a noticeable difference is observable from 0.7 THz. The blue and green solid

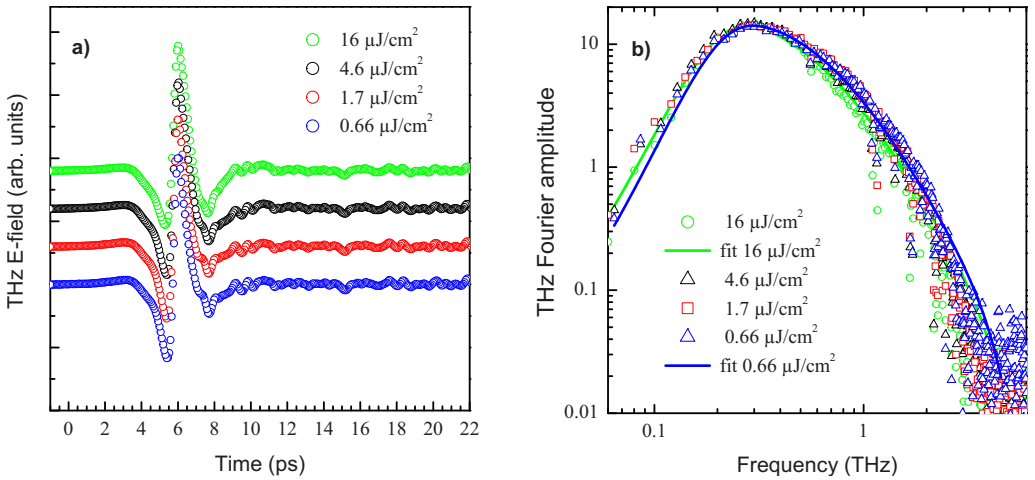

FIG. 2. (Color online) Normalized THz traces (a) and their corresponding spectra (b) obtained for different laser fluences on the THz emitter. The THz traces are displaced vertically for clarity. In (b) the THz spectra are plotted on a log-log scale in order to show the different break points of the instrumental response function. The solid lines plotted in (b) for laser fluences of 0.66 and 16 $\mu J/cm^2$ per pulse correspond to best fits of the data using the Eq. (8) with $\omega_{lf}/2\pi=0.17$ THz, $\Delta\omega_{lf}/2\pi=0.09$ THz, $\tau_s=200$ fs, and a $\alpha_{GaAs}(\omega)$ function taken from the absorption curve plotted in Fig. 1.

lines in Fig. 2(b) correspond to the best fits of the 0.66 and 16 $\mu J/cm^2$ experimental spectra, respectively, using Eq. (8). Several model parameters are fixed by experimental considerations, rather than being used as free parameters in the fitting procedure. Given the characteristics of our focusing Si lenses, the diameter of the diffraction-limited Airy disk on the detector[22] is about 300 μm at $f_o=0.17$ THz, which is 10 times the size of the gap between the electrodes of our detector. We, therefore, assumed a cut-off frequency of $\omega_{lf}/2\pi=0.17$ THz and width of $\Delta\omega_{lf}/2\pi=0.09$ THz for the low-frequency fall-off function, for all curves, which reproduces the data reasonably well; the fitting parameters ω_{lf} and $\Delta\omega_{lf}$ have almost no influence on the extracted carrier trapping time value, which is our main concern here. The absorption of THz radiation by the 1 mm thick GaAs material has been taken into account in the model using data of Fig. 1. The small discrepancies between the fit curves and the data points observed at high frequencies (>2.5 THz) might be due to a stronger absorption or to longer optical pathways for rays that pass through the GaAs substrate at oblique angles. Finally, the ultrafast scattering time (τ_s) parameter is difficult to obtain using this fitting procedure. Several groups have estimated the scattering time in semi-insulating GaAs and found values between 50 up to 270 fs, depending on the temperature and the photoexcitation conditions (see Markelz *et al.*[34]): for instance the presence of a nonequilibrium phonon population tends to decrease this scattering time. Figure 2(b) shows the best fits obtained for a fixed scattering time parameter of 200 fs. The carrier capture time by the traps (τ_c) and the proportionality constants are thus the only free parameters of this fitting procedure. The error bar on the carrier trapping time (τ_c) results from our inability to determine precisely the scattering time (τ_s) value. By considering a τ_s value of 200 ± 50 fs, the fitting procedure yields a carrier trapping time values of 0.54 ± 0.08 ps for a laser pump fluence of 0.66 $\mu J/cm^2$. For the fits of the spectra obtained at higher pump fluence on the emitter we have used a response function with a fixed 0.54 ps capture time for the detector (the value obtained at low fluence) and an adjustable parameter for the average capture time in the THz emitter. The slight increase of the carrier trapping time at the highest laser fluence might be explained by a partial filling of the traps situated near the GaAs surface of the emitter.[28]

Figure 3 shows the photocarrier dynamics measured in the visible-pump, THz probe experiment, as detected at the maximum field of the THz probe pulses. We plot the normalized differential transmission signal as a function of the pump-probe delay for three laser fluences. The solid lines correspond to the best fits of the data using the biexponential model in Eq. (9). The two extracted decay times (τ_{d1} and τ_{d2}) and the amplitude ratio of the two exponential decay components (A_2/A_1) are also shown. The first decay time, which is about 1.2 ps at low laser fluence, describes mainly the fast capture dynamics of the carriers generated in the ion-bombarded region of the substrate. The value of this short decay time seen in the pump-probe measurement is slightly larger than the one extracted from the instrumental Fourier

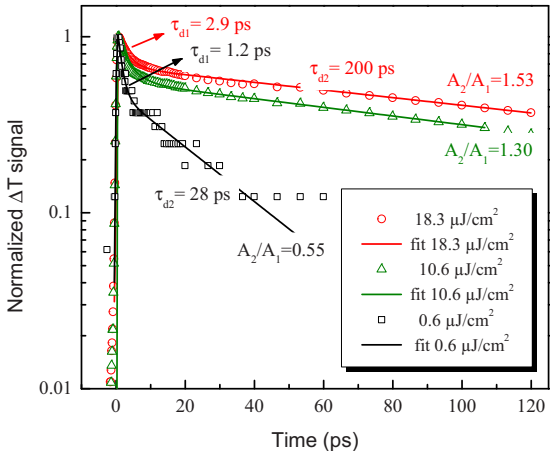

FIG. 3. (Color online) Normalized differential transmission signal detected at the maximum of the THz probe pulses and plotted as a function of the pump-probe delay. The time-resolved data curves are plotted for three laser fluences. The solid lines correspond to the best fits of the data using a biexponential model.

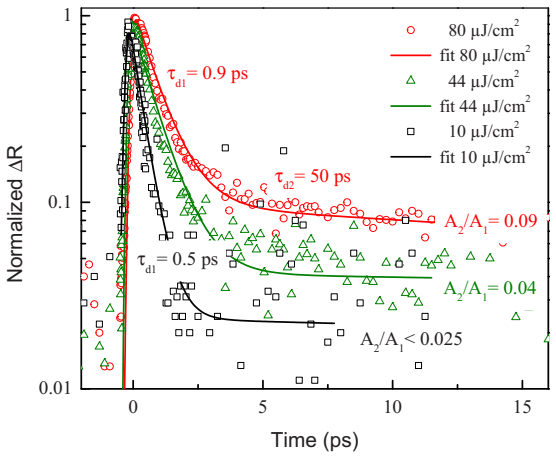

FIG. 4. (Color online) Normalized differential reflectivity signal obtained from a degenerate pump-probe experiment at 760 nm and plotted as a function of the pump-probe delay. The time-resolved data curves are plotted for three laser fluences. The solid lines correspond to the best fits of the data using a biexponential model.

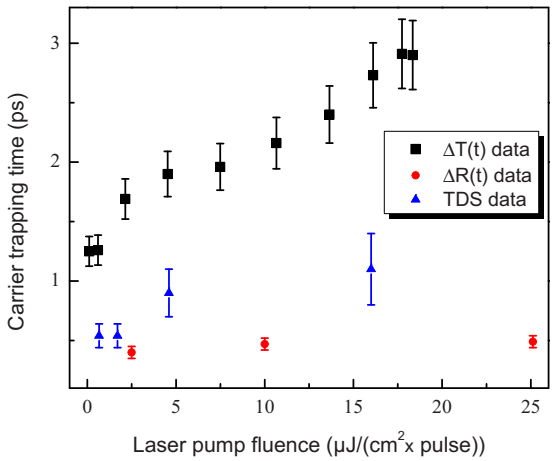

FIG. 5. (Color online) Comparison of the carrier trapping times extracted from the three experimental techniques for different laser pump fluences. The TDS data corresponds to those extracted from the instrumental response of our THz time-domain spectroscopy setup. All measurements are obtained at 300 K on the same ion-bombarded GaAs substrate.

response of our THz TDS setup. This likely indicates an enhanced sensitivity of the antenna response to the carrier density very near the surface, a consequence of the spatial distribution of the DC bias field between the electrodes. The surface carriers may recombine more rapidly than the ones that are generated over a 1 μm depth using the 820 nm pump beam. The second exponential decay component describes the dynamics of those carriers that are generated in or that reach the undamaged region of the GaAs substrate. The enhancement of A_2/A_1 with increased fluence indicates that more carriers are diffusing and recombining in the bulk of the GaAs substrate. This behavior may result from the filling of traps in the ion-bombarded layer. The bulk GaAs carrier recombination time is probably longer than 200 ps, which is the extracted value obtained at the highest laser fluence. At the lowest fluence, we observe a significant reduction of this long decay time. This behavior is explained by a reverse diffusion toward the surface of carriers generated in the bulk, once the initial distribution of carriers generated in the ion-damaged region disappears.

Figure 4 shows the normalized differential reflectivity signal obtained using a degenerate pump-probe experiment at 760 nm. Time-resolved data curves have been obtained for several laser fluences from 2.5 to 80 $\mu J/cm^2$ per pulse. We have plotted three of these time-resolved data curves in Fig. 4. The solid lines of this figure correspond to the best fits of the data using again the biexponential model of Eq. (9). The A_2/A_1 ratio is less significant at low laser fluences (<10 $\mu J/cm^2$ per pulse) because the signal to noise ratio is very small for delay times longer than 2 ps. As before, the short decay times is related to the fast capture mechanism of the photoexcited carriers by the traps that are present near the GaAs surface. These values are in good agreement with the times extracted from the analysis of the THz spectra of Fig. 1. We believe that both techniques probe the photocarrier density at the GaAs surface. The exact nature of the mechanisms that account for the second exponential observed in the time-resolved data curves of Fig. 4 is not known precisely: it might be due to in-depth diffusion and recombination processes but also to long-time thermal effect. Ratios of the two exponential decay components (A_2/A_1) are much smaller than those obtained for the time-resolved THz transmission curves, which indicate again that carrier capture by the traps present close to the GaAs surface governs the dynamics of these time-resolved reflectivity measurements.

The comparison of the carrier trapping times extracted from the three experimental techniques is summarized in Fig. 5. Both the pump-probe differential reflectivity technique and the THz-TDS Fourier analysis technique allow probing the ultrafast dynamics of those carriers that are photoexcited near the GaAs surface. A carrier trapping time of about 0.5 ps has been obtained at low laser pump fluences and the averaged carrier trapping time gets longer as the pump fluence increases. The carrier trapping times extracted from the 820 nm pump per THz probe technique are slightly slower than the values determined using the other two techniques but similar fluence-dependent trapping time behavior is observed. The THz differential transmission technique overestimates the carrier trapping time that governs the PC antenna characteristics since it probes the conductivity properties of the overall distribution of photoexcited carriers. This technique is, therefore, more sensitive to carrier diffusion and recombination mechanisms in the undamaged region of the ion-bombarded substrate. At a laser fluence of 10 $\mu J/cm^2$ per pulse, the amplitude ratio A_2/A_1 of the two exponential decay components, extracted from $\Delta T(t)$ data curves, is about 35 times higher than the one extracted from the $\Delta R(t)$ data curves.

V. CONCLUSION

In this work, we have developed a comprehensive model to obtain an analytical expression for the instrumental response of a time-domain spectrometer that integrates photoconductive transmitter and receiver antennas made on identical proton-bombarded GaAs substrates. It reproduces the instrumental response of our time-domain THz spectroscopy setup and the ultrafast capture time of the photoexcited car-

riers appears to be a key parameter of this model. A 0.5 ps capture time has been found at low pump fluences (<5 $\mu J/cm^2$ per pulse) and this time gets longer as the fluence increases. This behavior can be explained by a gradual filling of the traps that are distributed over a 1 μm depth from the GaAs surface. This interpretation is supported by time-resolved measurements obtained on the same photoconductive material using both an 820 nm pump/terahertz-probe transmission experiment and a degenerate 760 nm pump/probe reflectivity experiment. The strong correlation that has been established between these different measurements reinforces the theoretical model used to reproduce the instrumental response of this terahertz setup.

ACKNOWLEDGMENTS

This collaboration between Simon-Fraser University and Université de Sherbrooke was supported by CIFAR. This work was also supported financially by NSERC, CFI, FQRNT (Québec), and Nano-Québec. The authors would like to thank J. Beerens, M. Lacerte, P. Lafrance, S. Pelletier, G. Laliberté, and G. Bertrand for sample preparation and technical assistance.

[1] D. Grischkowsky, in *Springer Handbook of Lasers and Optics, Part D*, edited by F. Träger (Springer, New York, 2007), Chap. 17, pp. 1099–1152, 2007.
[2] D. Mittleman, *Sensing with Terahertz Radiation* (Springer, New York, 2003).
[3] M. van Exter and D. Grischkowsky, IEEE Trans. Microwave Theory Tech. **38**, 1684 (1990).
[4] S. Gupta, M. Y. Frankel, J. A. Yaldmanis, J. F. Whitaker, and G. A. Mourou, Appl. Phys. Lett. **59**, 3276 (1991).
[5] E. S. Harmon, M. R. Melloch, J. M. Woodall, D. D. Nolte, and N. Otsuka, Appl. Phys. Lett. **63**, 2248 (1993).
[6] S. Kono, M. Tani, and K. Sakai, Appl. Phys. Lett. **79**, 898 (2001).
[7] T.-A. Liu, M. Tani, and C.-L. Pan, J. Appl. Phys. **93**, 2996 (2003).
[8] Gong-Ru Lin and Ci-Ling Pan, Appl. Phys. B: Lasers Opt. **72**, 151 (2001).
[9] J. Lloyd-Hughes, E. Castro-Camus, M. D. Fraser, C. Jagadish, and M. B. Johnston, Phys. Rev. B **70**, 235330 (2004).
[10] B. Salem, D. Morris, V. Aimez, J. Beauvais, and D. Houde, Semicond. Sci. Technol. **21**, 283 (2006).
[11] B. Salem, D. Morris, Y. Salissou, V. Aimez, S. Charlebois, M. Chicoine, and F. Schiettekatte, J. Vac. Sci. Technol. A **24**, 774 (2006).
[12] P. Uhd Jepsen, R. H. Jacobsen, and S. R. Keiding, J. Opt. Soc. Am. B **13**, 2424 (1996).
[13] Z. Piao, M. Tani, and K. Sakai, Jpn. J. Appl. Phys., Part 1 **39**, 96 (2000).
[14] L. Duvillaret, F. Garet, J. F. Roux, and J. L. Coutaz, IEEE J. Sel. Top. Quantum Electron. **7**, 615 (2001).
[15] E. Castro-Camus, J. Lloyd-Hughes, and M. B. Johnston, Phys. Rev. B **71**, 195301 (2005).
[16] N. Chimot, J. Mangeney, L. Joulaud, P. Crozat, H. Bernas, K. Blary, and J. F. Lampin, Appl. Phys. Lett. **87**, 193510 (2005).
[17] R.-H. Chou, T.-A. Liu, and C.-L. Pan, J. Appl. Phys. **104**, 053121 (2008).
[18] S. Rihani, R. Faulks, H. Beere, H. Page, I. Gregory, M. Evans, D. A. Ritchie, and M. Pepper, Appl. Phys. Lett. **95**, 051106 (2009).
[19] S. Funk, G. Acuna, M. Handloser, and R. Kersting, Opt. Express **17**, 17450 (2009).
[20] D. H. Auston, K. P. Cheung, and P. R. Smith, Appl. Phys. Lett. **45**, 284 (1984).
[21] J. F. Corson, Ph.D. thesis, University of California at Berkeley, 2000.
[22] A. Bitzer, H. Helm, and M. Walther, IEEE J. Sel. Top. Quantum Electron. **14**, 476 (2008).
[23] G. C. Loata, M. D. Thomson, T. Löffler, and H. G. Roskos, Appl. Phys. Lett. **91**, 232506 (2007).
[24] D. Grischkowsky and N. Katzenellenbogen, in *OSA Proceedings on Picosecond Electronics and Optoelectronics*, edited by T. C. L. Sollner and J. Shah, OSA, Washington, D.C., 9–14 (1991).
[25] D. Grischkowsky, S. Keiding, M. van Exter, and Ch. Fattinger, J. Opt. Soc. Am. B **7**, 2006 (1990).
[26] Y. C. Shen, P. C. Upadhya, E. H. Linfield, H. E. Beere, and A. G. Davies, Appl. Phys. Lett. **83**, 3117 (2003).
[27] M. C. Beard, G. M. Turner, and C. A. Schmuttenmaer, Phys. Rev. B **62**, 15764 (2000).
[28] M. C. Beard, G. M. Turner, and C. A. Schmuttenmaer, J. Appl. Phys. **90**, 5915 (2001).
[29] D. G. Cooke, F. A. Hegmann, Yu. I. Mazur, Zh. M. Wang, W. Black, H. Wen, G. J. Salamo, T. D. Mishima, G. D. Lian, and M. B. Johnson, J. Appl. Phys. **103**, 023710 (2008).
[30] M. Lambsdorff, J. Kuhl, J. Rosenzweig, A. Axmann, and Jo. Schneider, Appl. Phys. Lett. **58**, 1881 (1991).
[31] S. Janz, U. G. Akano, and I. V. Mitchell, Appl. Phys. Lett. **68**, 3287 (1996).
[32] F. Ganikhanov, G.-R. Lin, W.-C. Chen, C.-S. Chang, and C.-L. Pana, Appl. Phys. Lett. **67**, 3465 (1995).
[33] V. Ortiz, J. Nagle, and A. Alexandrou, Appl. Phys. Lett. **80**, 2505 (2002).
[34] A. G. Markelz and E. J. Heilweil, Appl. Phys. Lett. **72**, 2229 (1998).